

Massive neutron stars with hyperonic core : a case study with the IUFSU model

Bipasha Bhowmick,^{*} Madhubrata Bhattacharya,[†] Abhijit Bhattacharyya,[‡] and G. Gangopadhyay[§]

*Department of Physics, University of Calcutta,
92 Acharya Prafulla Chandra Road,
Kolkata-700 009, India*

The recent discoveries of massive neutron stars, such as PSR J0348+0432 and PSR J1614–2230, have raised questions about the existence of exotic matter such as hyperons in the neutron star core. The validity of many established equations of states (EoS's) like the GM1 and FSUGold are also questioned. We investigate the existence of hyperonic matter in the central regions of massive neutron stars using Relativistic Mean Field (RMF) theory with the recently proposed IUFSU model. The IUFSU model is extended by including hyperons to study the neutron star in β equilibrium. The effect of different hyperonic potentials, namely Σ and Ξ potentials, on the EoS and hence the maximum mass of neutron stars has been studied. We have also considered the effect of stellar rotation since the observed massive stars are pulsars. It has been found that a maximum mass of $1.93M_{\odot}$, which is within the 3σ limit of the observed mass of PSR J0348 + 0432, can be obtained for rotating stars, with certain choices of the hyperonic potentials. The said star contains a fair amount of hyperons near the core.

PACS numbers: 21.30.Fe, 26.60.-c, 21.80.+a

I. INTRODUCTION

The recent discoveries of the massive neutron stars PSR J0348 + 0432 [1] and PSR J1614 – 2230 [2] have brought new challenges for theories of dense matter beyond the nuclear saturation density. Recently the radio timing measurements of the pulsar PSR J0348 + 0432 and its white dwarf companion have confirmed the mass of the pulsar to be in the range of $1.97 - 2.05 M_{\odot}$ at 68.27% or $1.90 - 2.18 M_{\odot}$ at 99.73% confidence [1]. This is only the second neutron star (NS) with a precisely determined mass around $2M_{\odot}$, after PSR J1614 – 2230 and has a 3σ lower mass limit $0.05 M_{\odot}$ higher than the latter. It therefore provides the tightest reliable lower bound on the maximum mass of neutron stars.

Compact stars provide the perfect astrophysical environment for testing theories of cold and dense matter. Densities at the core of neutron stars can reach values of several times of $10^{15} gm cm^{-3}$. At such high densities, the energies of the particles are high enough to favour the appearance of exotic particles in the core. Since the lifetime of neutron stars are much greater than those associated with the weak interaction, strangeness conservation can be violated in the core due to the weak interaction. This would result in the appearance of strange particles such as hyperons. The appearance of such particles produces new degrees of freedom, which results in a softer equation of state (EoS) in the neutron star interior.

The observable properties of compact stars depend crucially on the EoS. According to the existing models of

dense matter the presence of strangeness in the neutron star interior leads to a considerable softening of the EoS, resulting in a reduction of the maximum mass of the neutron star [3–6]. Therefore many existing theories involving hyperons cannot explain the large pulsar masses [7]. Most relativistic models obtain maximum neutron star masses in the range $1.4 - 1.8M_{\odot}$ [8–15], when hyperons are included. Some authors have tackled this problem by including a strong vector repulsion in the strange sector or by pushing the threshold for the appearance of hyperons to higher densities [15–22]. In several studies the maximum neutron star masses were generally found to be lower than $1.6M_{\odot}$ [4–6, 23–27] which is in contradiction with observed pulsar masses. However, neutron stars with maximum mass larger than $2M_{\odot}$ have been obtained theoretically. Bednarek *et al.* [28] achieved a stiffening of the EoS by using a non-linear relativistic mean field (RMF) model with quartic terms involving the strange vector meson. Lastowiecki *et al.* [29] obtained massive stars including a quark matter core. Taurines *et al.* [30] achieved large neutron star masses including hyperons by considering a model with density dependent coupling constants. The coupling constants were varied nonlinearly with the scalar field. Bonanno and Sedrakian [31] also modeled massive neutron stars including hyperons and quark core using a fairly stiff EoS and vector repulsion among quarks. Authors in ref. [32] incorporated higher order couplings in the RMF theory in addition to kaonic interactions to obtain the maximum neutron star mass. Agrawal *et al.* [33] have optimized the parameters of the extended RMF model using a selected set of global observables which includes binding energies and charge radii for nuclei along several isotopic and isotonic chains and the iso-scalar giant monopole resonance energies for the ^{90}Zr and ^{208}Pb nuclei. Weissenborn *et al.* [34] investigated the vector meson-hyperon coupling, going from SU(6) quark model to a broader SU(3), and

^{*}Electronic address: bips.gini@gmail.com

[†]Electronic address: madhubrata.b@rediffmail.com

[‡]Electronic address: abphy@caluniv.ac.in

[§]Electronic address: ggphy@caluniv.ac.in

concluded that the maximum mass of a neutron star decreases linearly with the strangeness content of the neutron star core independent of the nuclear EoS. On the other hand, H. Dapo *et al.* [6] found that for several different bare hyperon-nucleon potentials and a wide range of nuclear matter parameters the hyperons in neutron stars are always present.

The parameters of the RMF model are fitted to the saturation properties of the infinite nuclear matter and/or the properties of finite nuclei. As a result extrapolation to higher densities and asymmetry involve uncertainties. Three of these properties of the infinite nuclear matter are more precisely known: (a) the saturation density, (b) the binding energy and (c) the asymmetry energy, compared to the remaining ones - the effective nucleon mass and the compression modulus of the nuclear matter. The uncertainty in the dense matter EoS is basically related to the uncertainty in these two saturation properties. It has been seen that to reproduce the giant monopole resonance (GMR) in ^{208}Pb , accurately fitted non-relativistic and relativistic models predict compression modulus in the symmetric nuclear matter (K) that differ by about 25%. The reason for this discrepancy being the density dependence of the symmetry energy. Moreover, the alluded correlation between K and the density dependence of the symmetry energy results in an underestimation of the frequency of oscillations of neutrons against protons, the so-called isovector giant dipole resonance (IVGDR) in ^{208}Pb . FSUGold is a recently proposed accurately calibrated relativistic parameterization. It simultaneously describes the GMR in ^{90}Zr and ^{208}Pb and the IVGDR in ^{208}Pb without compromising the success in reproducing the ground-state observables [35]. The main virtue of this parameterization is the softening of both the EoS of symmetric nuclear matter and the symmetry energy. This softening appears to be required for an accurate description of different collective modes having different neutron-to-proton ratios. As a result, the FSUGold effective interaction predicts neutron star radii that are too large and a maximum stellar mass that is too small [36].

The Indiana University-Florida State University (IUFUSU) interaction, is a new relativistic parameter set,

derived from FSUGold. It is simultaneously constrained by the properties of finite nuclei, their collective excitations and the neutron star properties by adjusting two of the parameters of the theory - the neutron skin thickness of ^{208}Pb and the maximum neutron star mass [37]. As a result the new effective interaction softens the EoS at intermediate densities and stiffens the EoS at high density. As it stands now, the new IUFUSU interaction reproduces the binding energies and charge radii of closed-shell nuclei, various nuclear giant (monopole and dipole) resonances, the low-density behavior of pure neutron matter, the high-density behavior of the symmetric nuclear matter and the mass-radius relationship of neutron stars. Whether this new EoS can accommodate the hyperons inside the compact stars, with the severe constraints imposed by the recent observations of $\sim 2M_\odot$ pulsars, needs to be explored. In this work we plan to make a detailed study of such a possibility. For this purpose we have extended the IUFUSU interaction by including the full baryon octet. A new EoS is constructed to investigate the neutron star properties with hyperons.

The paper is organized as follows. In section 2, we briefly discuss the model used and the resulting EoS. In the next section we use this EoS to look at static and rotating star properties. We give a brief summary in section 4.

II. IUFUSU WITH HYPERONS

One of the possible approaches to describe neutron star matter is to adopt an RMF model subject to β equilibrium and charge neutrality. For our investigation of nucleons and hyperons in the compact star matter we choose the full standard baryon octet as well as electrons and muons. Contribution from neutrinos are not taken into account assuming that they can escape freely from the system. In this model, baryon-baryon interaction is mediated by the exchange of scalar (σ), vector (ω), isovector (ρ) and the strange vector (ϕ) mesons. The Lagrangian density we consider is given by [37]

$$\begin{aligned} \mathcal{L} = & \sum_B \bar{\psi}_B [i\gamma^\mu \partial_\mu - m_B + g_{\sigma B}\sigma - g_{\omega B}\gamma^\mu \omega_\mu - g_{\phi B}\gamma^\mu \phi_\mu - \frac{g_{\rho B}}{2}\gamma^\mu \vec{\tau} \cdot \vec{\rho}^\mu] \psi_B + \frac{1}{2}\partial_\mu \sigma \partial^\mu \sigma - \frac{1}{2}m_\sigma^2 \sigma^2 \\ & - \frac{\kappa}{3!}(g_{\sigma N}\sigma)^3 - \frac{\lambda}{4!}(g_{\sigma N}\sigma)^4 - \frac{1}{4}F_{\mu\nu}F^{\mu\nu} + \frac{1}{2}m_\omega^2 \omega_\mu \omega^\mu + \frac{\zeta}{4!}(g_{\omega N}\omega_\mu \omega^\mu)^2 + \frac{1}{2}m_\rho^2 \vec{\rho}_\mu \cdot \vec{\rho}^\mu - \frac{1}{4}\vec{G}_{\mu\nu}\vec{G}^{\mu\nu} \\ & + \Lambda_v(g_{\rho N}\vec{\rho}_\mu \cdot \vec{\rho}^\mu)(g_{\omega N}\omega_\mu \omega^\mu) + \frac{1}{2}m_\phi^2 \phi_\mu \phi^\mu - \frac{1}{4}H_{\mu\nu}H^{\mu\nu} + \sum_l \bar{\psi}_l [i\gamma^\mu \partial_\mu - m_l] \psi_l \end{aligned} \quad (1)$$

where the symbol B stands for the baryon octet (p , n , Λ , Σ^+ , Σ^0 , Σ^- , Ξ^- , Ξ^0) and l represents e^- and μ^- .

The masses m_B , m_σ , m_ω , m_ρ and m_ϕ are respectively for baryon, σ , ω , ρ and ϕ mesons. The antisymmetric tensors

Model	$g_{\sigma n}^2$	$g_{\omega n}^2$	$g_{\rho n}^2$	κ (MeV)	λ	ζ	Λ_v
FSU	112.1996	204.5469	138.4701	1.4203	0.023762	0.06	0.030
IUFSU	99.4266	169.8349	184.6877	3.3808	0.000296	0.03	0.046

TABLE I: Parameter sets for the two models discussed in the text. The nucleon mass and the meson masses are kept fixed at $m_n = 939$ MeV, $m_\sigma = 491.5$ MeV, $m_\omega = 782.5$ MeV, $m_\rho = 763$ MeV and $m_\phi = 1020$ MeV in both the models.

of vector mesons take the forms $F_{\mu\nu} = \partial_\mu\omega_\nu - \partial_\nu\omega_\mu$, $G_{\mu\nu} = \partial_\mu\vec{\rho}_\nu - \partial_\nu\vec{\rho}_\mu + g[\vec{\rho}_\mu, \vec{\rho}_\nu]$ and $H_{\mu\nu} = \partial_\mu\phi_\nu - \partial_\nu\phi_\mu$. The isoscalar meson self-interactions (via κ , λ and ζ terms) are necessary for the appropriate EoS of the symmetric nuclear matter [38]. The new additional isoscalar-isovector coupling (Λ_v) term is used to modify the density dependence of the symmetry energy and the neutron-skin thickness of heavy nuclei [36, 37]. The meson-baryon coupling constants are given by $g_{\sigma B}$, $g_{\omega B}$, $g_{\rho B}$ and $g_{\phi B}$.

All the nucleon-meson parameters used in this work are shown in Table I. The saturation properties of the symmetric nuclear matter produced by IUFSU are: saturation density $n_0 = 0.155$ $f m^{-3}$, binding energy per nucleon $\varepsilon_0 = -16.40$ MeV and compression modulus $K = 231.2$ MeV.

The hyperon-meson couplings are taken from the SU(6) quark model [39, 40] as,

$$\begin{aligned} g_{\rho\Lambda} &= 0, \quad g_{\rho\Sigma} = 2g_{\rho\Xi} = 2g_{\rho N} \\ g_{\omega\Lambda} &= g_{\omega\Sigma} = 2g_{\omega\Xi} = \frac{2}{3}g_{\omega N} \\ 2g_{\phi\Lambda} &= 2g_{\phi\Sigma} = g_{\phi\Xi} = \frac{-2\sqrt{2}}{3}g_{\omega N} \end{aligned}$$

The scalar couplings are determined by fitting the hyperonic potential,

$$U_Y^{(N)} = g_{\omega Y}\omega_0 + g_{\sigma Y}\sigma_0 \quad (2)$$

where Y stands for the hyperon and σ_0 , ω_0 are the values of the scalar and vector meson fields at saturation density [9]. The values of $U_Y^{(N)}$ are taken from the available hypernuclear data. The best known hyperonic potential is that of Λ , having a value of about $U_\Lambda^{(N)} = -30$ MeV [41]. In case of Σ and Ξ hyperons, the potential depths are not as clearly known as in the case of Λ . However, analyses of laboratory experiments indicate that at nuclear densities the Λ -nucleon potential is attractive but the Σ^-

-nucleon potential is repulsive [42]. Therefore, we have varied both $U_\Sigma^{(N)}$ and $U_\Xi^{(N)}$ in the range of -40 MeV to +40 MeV to investigate the properties of neutron star matter.

For neutron star matter, with baryons and charged leptons, the β -equilibrium conditions are guaranteed with the following relations between chemical potentials for different particles:

$$\begin{aligned} \mu_p &= \mu_{\Sigma^+} = \mu_n - \mu_e \\ \mu_\Lambda &= \mu_{\Sigma^0} = \mu_{\Xi^0} = \mu_n \\ \mu_{\Sigma^-} &= \mu_{\Xi^-} = \mu_n + \mu_e \\ \mu_\mu &= \mu_e \end{aligned} \quad (3)$$

and the charge neutrality condition is fulfilled by

$$n_p + n_{\Sigma^+} = n_e + n_{\mu^-} + n_{\Sigma^-} + n_{\Xi^-} \quad (4)$$

where n_i is the number density of the i 'th particle. The effective chemical potentials of baryons and leptons can be given by

$$\mu_B = \sqrt{k_F^B{}^2 + m_B^{*2}} + g_{\omega B}\omega + g_{\rho B}\tau_3 B\rho \quad (5)$$

$$\mu_l = \sqrt{K_F^l{}^2 + m_l^2} \quad (6)$$

where $m_B^* = m_B - g_{\sigma B}\sigma$ is the baryon effective mass and K_F^l is the Fermi momentum of the lepton (e , μ). The EoS of neutron star matter can be given by,

$$\begin{aligned} \varepsilon &= \frac{1}{2}m_\sigma^2\sigma^2 + \frac{\kappa}{6}g_{\sigma N}^3\sigma^3 + \frac{\lambda}{24}g_{\sigma N}^4\sigma^4 + \frac{1}{2}m_\omega^2\omega^2 + \frac{\zeta}{8}g_{\omega N}^4\omega^4 + \frac{1}{2}m_\rho^2\rho^2 + 3\Lambda_v g_{\rho N}^2 g_{\omega N}^2 \omega^2 \rho^2 \\ &+ \frac{1}{2}m_\phi^2\phi^2 + \sum_B \frac{\gamma_B}{(2\pi)^3} \int_0^{k_F^B} \sqrt{k^2 + m_B^{*2}} d^3k + \frac{1}{\pi^2} \sum_l \int_0^{K_F^l} \sqrt{k^2 + m_l^2} k^2 dk \end{aligned} \quad (7)$$

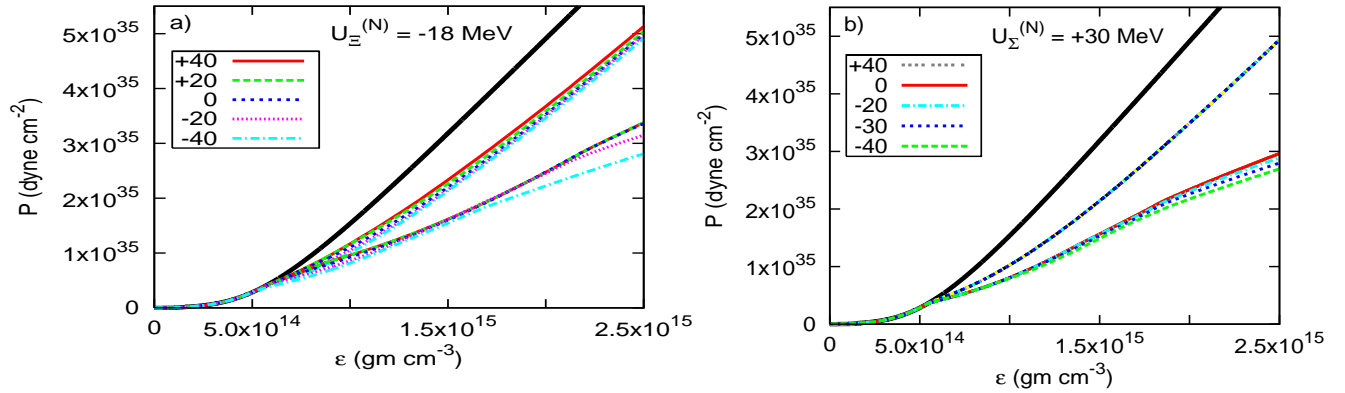


FIG. 1: (color online) a) EoS obtained with varying $U_{\Sigma}^{(N)}$ at fixed $U_{\Xi}^{(N)}$. The upper branch shows the EoS for a system containing nucleons, leptons and all the non strange mesons. The middle branch shows the EoS for a system containing the whole baryon octet, the leptons and σ , ω , ρ and ϕ mesons. The lower branch shows the EoS for the particles contained in the middle branch except ϕ . b) EoS obtained with varying $U_{\Xi}^{(N)}$ at fixed $U_{\Sigma}^{(N)}$. The compositions of the upper, middle and lower branches are same as those of a) respectively.

$$\begin{aligned}
 P = & -\frac{1}{2}m_{\sigma}^2\sigma^2 - \frac{\kappa}{6}g_{\sigma N}^3\sigma^3 - \frac{\lambda}{24}g_{\sigma N}^4\sigma^4 + \frac{1}{2}m_{\omega}^2\omega^2 + \frac{\zeta}{24}g_{\omega N}^4\omega^4 + \Lambda_v g_{\rho N}^2 g_{\omega N}^2 \omega^2 \rho^2 + \frac{1}{2}m_{\rho}^2\rho^2 \\
 & + \frac{1}{2}m_{\phi}^2\phi^2 + \frac{1}{3}\sum_B \frac{\gamma_B}{(2\pi)^3} \int_0^{k_F^B} \frac{k^2 d^3k}{(k^2 + m_B^{*2})^{1/2}} + \frac{1}{3}\sum_l \frac{1}{\pi^2} \int_0^{K_F^l} \frac{k^4 dk}{(k^2 + m_l^2)^{1/2}}
 \end{aligned} \tag{8}$$

where ε and P stand for energy density and pressure respectively and γ_B is the baryon spin-isospin degeneracy factor.

In fig. 1 we plot the EoS for different values of the hyperonic potentials. The upper branch is for the usual nuclear matter which does not contain any strange particle. The middle and lower branches are for full baryon octet, leptons and σ , ω , ρ mesons. In addition, the middle branch contains the ϕ meson. In the left panel, *i.e.* in fig. 1a, we keep $U_{\Xi}^{(N)}$ fixed at -18 MeV, this value is generally adopted from hypernuclear experimental data [43]. For the middle and lower branches we vary the Σ potential from -40 MeV to +40 MeV in steps of 20 MeV. The lower branch shows that for an attractive Σ potential the EoS gets stiffer as $U_{\Sigma}^{(N)}$ increases. However as $U_{\Sigma}^{(N)}$ becomes positive the EoS seems to become independent of $U_{\Sigma}^{(N)}$. We see from fig. 1a that for $U_{\Sigma}^{(N)} > 0$ MeV the EoS remains identical to that for $U_{\Sigma}^{(N)} = 0$ MeV. However, once we add ϕ meson to the system, the EoS continues to get stiffer as $U_{\Sigma}^{(N)}$ moves to more positive side (middle branch of fig. 1a).

We then fix $U_{\Sigma}^{(N)}$ and vary $U_{\Xi}^{(N)}$. This is represented in fig. 1b, where we have fixed the value of $U_{\Sigma}^{(N)} = +30$ MeV (adopted from hypernuclear experi-

mental data [43]). We vary $U_{\Xi}^{(N)}$ from -40 MeV to +40 MeV. We see that for the lower branch, *i.e.* the case without the ϕ meson, the EoS gets stiffer with the increase in Ξ potential up to $U_{\Xi}^{(N)} = 0$ MeV. However, for positive values of $U_{\Xi}^{(N)}$ the EoS remains unchanged. Adding an extra repulsion to the system by including the ϕ meson changes the scenario altogether. The EoS becomes totally independent of the Ξ potential (middle branch of fig. 1b). From figures 1a and 1b one can generally conclude that the inclusion of ϕ meson makes the EoS stiffer, however, hyperonic EoS is much softer than the usual nuclear matter EoS.

In fig. 2 we have plotted the particle fractions for an attractive Σ potential $U_{\Sigma}^{(N)} = -30$ MeV and a repulsive potential $U_{\Sigma}^{(N)} = +30$ MeV keeping $U_{\Xi}^{(N)}$ fixed at -18 MeV, with and without ϕ in each case. From fig. 2a, when ϕ is not present, we see that all the hyperons contribute to the particle fractions for an attractive Σ potential whereas for repulsive $U_{\Sigma}^{(N)}$ there is no Σ present in the matter (fig. 2b). The appearance of Λ is also pushed to higher density compared to the case of an attractive potential. When ϕ is included in the system Σ^0 and Σ^- appear with Λ for $U_{\Sigma}^{(N)} = -30$ MeV (fig. 2c). However, for $U_{\Sigma}^{(N)} = +30$ MeV (fig. 2d), the threshold of Σ^- is pushed to higher density compared to the case

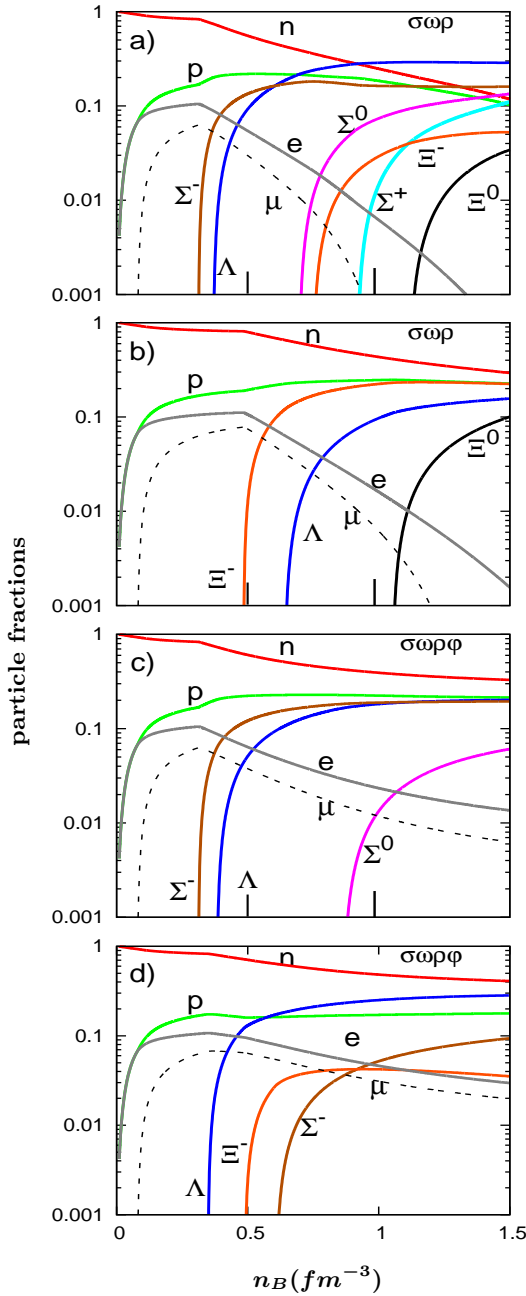


FIG. 2: (color online) Particle fractions for different Σ potential depths: a) for “ $\sigma\omega\rho$ ” with $U_{\Sigma}^{(N)} = -30$ MeV, b) for “ $\sigma\omega\rho$ ” with $U_{\Sigma}^{(N)} = +30$ MeV, c) for “ $\sigma\omega\rho\phi$ ” with $U_{\Sigma}^{(N)} = -30$ MeV, d) for “ $\sigma\omega\rho\phi$ ” with $U_{\Sigma}^{(N)} = +30$ MeV. $U_{\Xi}^{(N)}$ is fixed at -18 MeV in each case.

of $U_{\Sigma}^{(N)} = -30$ MeV, Σ^0 disappears and Ξ^- appears in the system. We also note that in the case of attractive Σ potential, Σ^- is always the first hyperon to appear in the system. For repulsive $U_{\Sigma}^{(N)}$, Ξ^- appears before others in the “ $\sigma\omega\rho$ ” case and Λ is the the first hyperon to appear in case of “ $\sigma\omega\rho\phi$ ”.

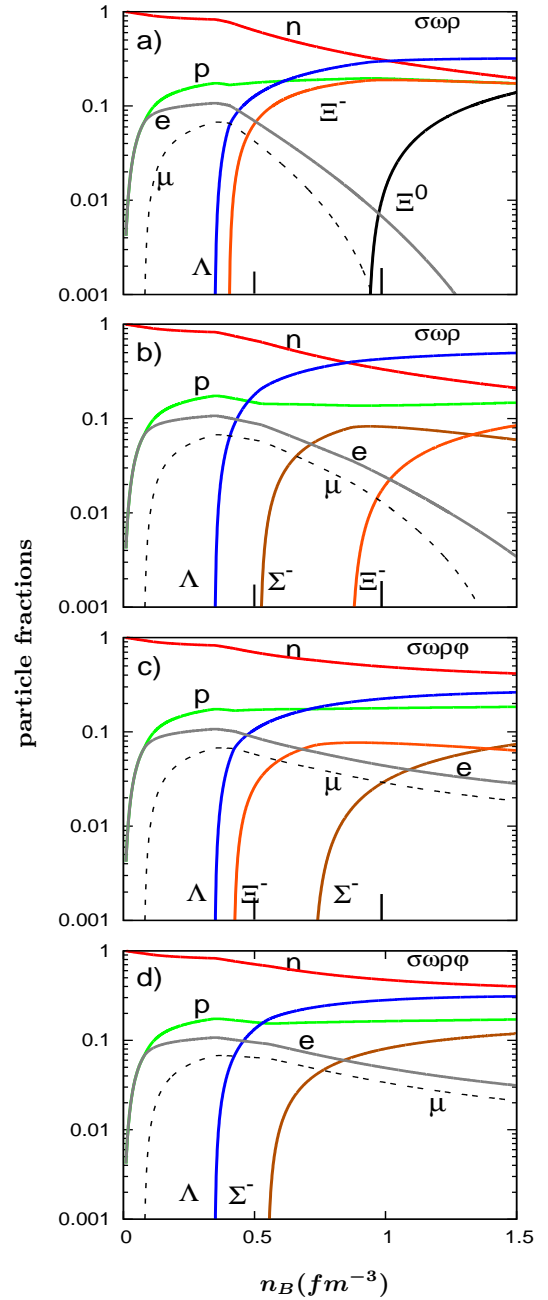


FIG. 3: (color online) Particle fractions for different Ξ potential depths: a) for “ $\sigma\omega\rho$ ” with $U_{\Xi}^{(N)} = -30$ MeV, b) for “ $\sigma\omega\rho$ ” with $U_{\Xi}^{(N)} = +30$ MeV, c) for “ $\sigma\omega\rho\phi$ ” with $U_{\Xi}^{(N)} = -30$ MeV, d) for “ $\sigma\omega\rho\phi$ ” with $U_{\Xi}^{(N)} = +30$ MeV. $U_{\Sigma}^{(N)}$ is fixed at $+30$ MeV in each case.

From fig. 2 we see that for negative values of $U_{\Sigma}^{(N)}$, the Σ 's are bound in matter and the effective mesonic interaction would be more attractive as the potential gets deeper. As a result, the EoS gets softer with more attractive $U_{\Sigma}^{(N)}$ (see fig. 1a). For $U_{\Sigma}^{(N)} \geq 0$, Σ 's are no longer bound to matter and the effective mesonic inter-

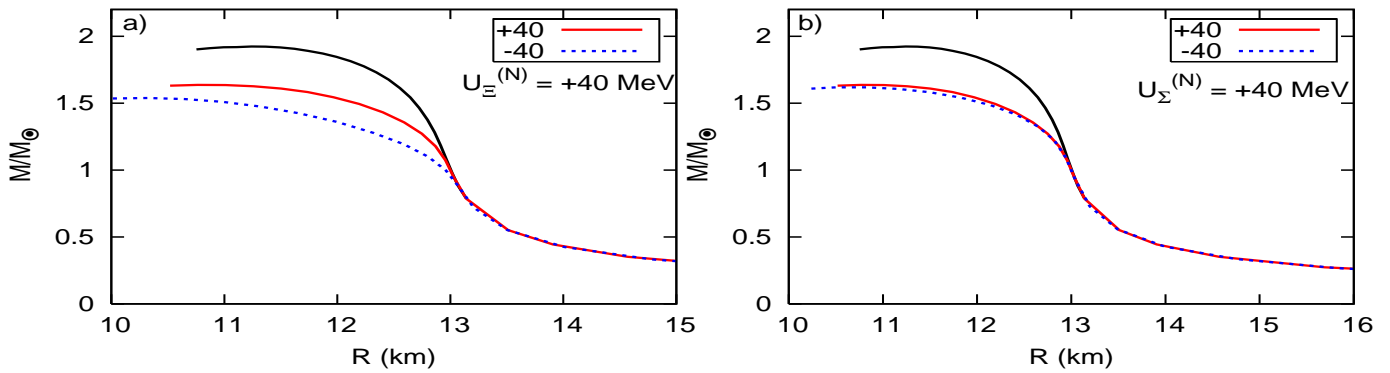


FIG. 4: (color online) Mass-radius curves for static star fixing the a) Ξ potential depth at $U_{\Xi}^{(N)} = +40$ MeV and varying the $U_{\Sigma}^{(N)}$. b) Σ potential depth at $U_{\Sigma}^{(N)} = +40$ MeV and varying the $U_{\Xi}^{(N)}$. The uppermost curve in each case corresponds to the pure nuclear matter.

action becomes more and more repulsive with increasing $U_{\Sigma}^{(N)}$. This should, in principle, stiffen the EoS. However, for the “ $\sigma\omega\rho$ ” case, up to neutron star densities, *i.e.* about $n_B \lesssim (4-7)n_0$, Σ 's are not present in the matter when the potential is repulsive and hence the EoS up to these densities becomes insensitive to $U_{\Sigma}^{(N)}$.

In fig. 3 the particle fractions are plotted for an attractive Ξ potential $U_{\Xi}^{(N)} = -30$ MeV and a repulsive potential $U_{\Xi}^{(N)} = +30$ MeV keeping $U_{\Sigma}^{(N)}$ fixed at +30 MeV. We see that in the first case *i.e.* when ϕ is not present and the potential is attractive (fig. 3a), all the hyperons except Σ 's are present in the system and the Λ hyperon dominates. When the Ξ potential becomes positive (fig. 3b) Ξ^0 disappears and the threshold for appearance of Ξ^- shifts to much higher density. However Σ^- is present in matter in this potential and it appears before Ξ^- . When ϕ is introduced in the system, for an attractive Ξ potential (fig. 3c), again Σ^- and Ξ^- are present along with Λ . However, the difference from fig. 3b *i.e.* “ $\sigma\omega\rho$ ” case and $U_{\Xi}^{(N)} \geq 0$ is that, here Ξ^- appears much before Σ^- . In the last case (fig. 3d), we see that as a result of the combined effects of inclusion of ϕ and repulsive potentials, only the Λ and Σ^- are present in the system. From both figures 2 and 3, we see that, inclusion of ϕ meson decreases the density of hyperons. Since ϕ is a strange particle, further strangeness is suppressed and as a result the hyperon densities are reduced compared to the “ $\sigma\omega\rho$ ” case.

III. STATIC AND ROTATING STARS

In this section we are going to discuss the properties of static and rotating axisymmetric stars using the EoS which we have studied in the last section. The EoS without ϕ meson is softer compared to that with ϕ meson. So we do not discuss the EoS without ϕ as it results in less maximum mass.

The stationary, axisymmetric space-time used to model the compact stars are defined through the metric

$$ds^2 = -e^{\gamma+\rho} dt^2 + e^{2\alpha} (dr^2 + r^2 d\theta^2) + e^{\gamma-\rho} r^2 \sin^2\theta (d\phi - \omega dt)^2 \quad (9)$$

where α , γ , ρ and ω are the gravitational potentials which depend on r and θ only.

In this work we adopt the procedure of Komatsu *et al.* [44] to look into the observable properties of static and rotating stars. Einstein's equations for the three gravitational potentials γ , ρ and ω can be solved using Green's function technique. The fourth potential α can be determined using these three potentials. Once these potentials are determined one can calculate all the observable quantities using those. The solution of the potentials and hence the determination of physical quantities is numerically quite an involved process. For this purpose the “rns” code [45] is used in this work. This code, developed by Stergoilas, is very efficient in calculating the rotating star observables.

We discuss the properties of static stars first. In fig. 4 we have plotted the mass-radius curves of static stars using the EoS with “ $\sigma\omega\rho\phi$ ”. A plot for the pure nuclear matter case is also given for comparison (uppermost curve of both the panels). The maximum mass of pure nuclear matter star in the static case is $1.92M_{\odot}$ with a radius of 11.24 km. We have found that the mass of hyperonic star becomes maximum for $U_{\Sigma}^{(N)} = +40$ MeV and $U_{\Xi}^{(N)} \geq 0$ MeV. Hence in fig. 4 and fig. 5 we have shown the effect of these potentials on the maximum mass of neutron stars by fixing one of the potentials at +40 MeV and varying the other. The left panel, *i.e.* fig. 4a, corresponds to $U_{\Xi} = +40$ MeV and U_{Σ} varying from -40 MeV to +40 MeV. In the right panel, *i.e.* in fig. 4b, it is the other way round. From fig. 4a one can see that the maximum mass of the star increases with $U_{\Sigma}^{(N)}$. For $U_{\Sigma}^{(N)} = +40$ MeV the maximum mass is $1.62M_{\odot}$ with a

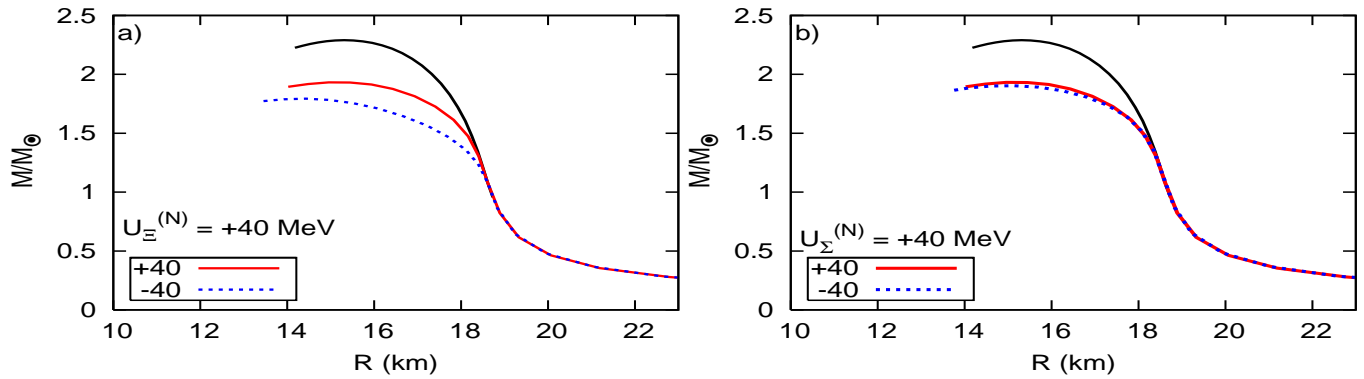


FIG. 5: (color online) Mass-radius curves for rotating stars for two cases: a) $U_{\Xi}^{(N)} = +40$ MeV and $-40 \text{ MeV} \leq U_{\Sigma}^{(N)} \leq +40$ MeV and b) $U_{\Sigma}^{(N)} = +40$ MeV and $-40 \text{ MeV} \leq U_{\Xi}^{(N)} \leq +40$ MeV. The uppermost curve in each case corresponds to the pure nuclear matter.

radius of 10.82 km. The central energy density of such a star is $\epsilon_c = 2.46 \times 10^{15} \text{ gm cm}^{-3}$. This is a reflection of the EoS shown in fig. 1a, which shows that the EoS becomes stiffer with increase in $U_{\Sigma}^{(N)}$. However, as seen from fig. 4b, the maximum mass of static stars is insensitive to $U_{\Xi}^{(N)}$, which should be obvious from fig. 1b as the EoS is independent of the cascade potential. Furthermore, from fig. 3d one can see that there is no cascade present in the medium. So the insensitivity of the EoS and hence the maximum mass, towards the cascade potential is expected. One should note that the maximum mass we obtain for the static stars is less than the observed mass of PSR J0348+0432. So the static stars with hyperons in the IUFSU parameter set can not incorporate a maximum mass $\sim 2M_{\odot}$. This result is consistent with the findings in Ref. [46]. However, since both of the observed $\sim 2M_{\odot}$ stars are pulsars, it would be a better idea to compare the observations with results from the rotating stars, which we do in the next part.

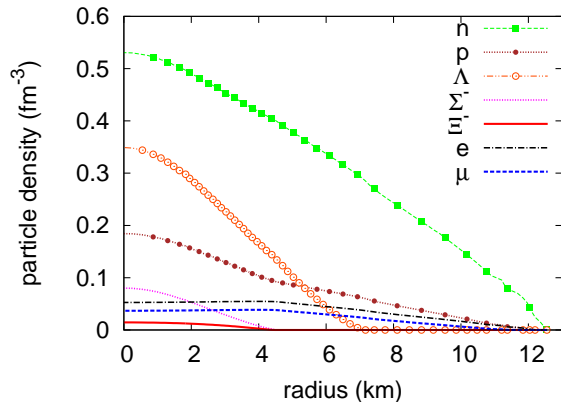


FIG. 6: (color online) Particle densities varying with radius along the equator. The potential depths for which particle densities are plotted are $U_{\Xi}^{(N)} = 0$ and $U_{\Sigma}^{(N)} = +40$ MeV.

In fig. 5 we plot the mass-radius curves for stars rotating with Keplerian velocities, for two cases. In fig. 5a we fix the cascade potential at $U_{\Xi}^{(N)} = +40$ MeV and vary $U_{\Sigma}^{(N)}$ from -40 MeV to $+40$ MeV. In fig. 5b it is the other way round. The pure nuclear matter case is also shown in the uppermost curve. The maximum mass for the pure nucleonic star is $2.29M_{\odot}$ with a radius of 15.31 km. We see that the maximum mass obtained for a rotating star with hyperonic core is $1.93M_{\odot}$ with a radius of 14.7 km in the Keplerian limit with angular velocity $\Omega = 0.86 \times 10^4 \text{ s}^{-1}$, for $U_{\Sigma}^{(N)} = +40$ MeV and $U_{\Xi}^{(N)} \geq 0$. As in the case of static sequence, we see that the maximum mass for the rotating case also increases with $U_{\Sigma}^{(N)}$ as we go towards more positive values of this potential. At $U_{\Sigma}^{(N)} = -40$ MeV we get a maximum mass of $1.79M_{\odot}$ whereas for $U_{\Sigma}^{(N)} = +40$ MeV the maximum mass is $1.93M_{\odot}$. The effect of $U_{\Xi}^{(N)}$ is much less significant on the maximum mass. From $U_{\Xi}^{(N)} = -40$ MeV to $U_{\Xi}^{(N)} = +40$ MeV mass is changed only by $\Delta M = 0.03M_{\odot}$.

In order to have a look at the composition of the maximum mass star, we have plotted the particle densities as a function of radius along the equator in fig. 6. For $U_{\Xi}^{(N)} = 0$ and $U_{\Sigma}^{(N)} = +40$ MeV, we see that a fair amount of hyperons are present in the core. There are Λ , Σ^- and Ξ^- present. Another interesting observation is that near the core, the density of Λ is much more compared to that of protons and it continues up to a distance of about 5 km from the center.

IV. SUMMARY AND CONCLUSIONS

To summarize, we have studied the static and rotating axisymmetric stars with hyperons using IUFSU model. The original FSUGold parameter set has been very successful in describing the properties of finite nuclei. With the discovery of highly massive neutron stars the rela-

bility of this model was questioned. It was then revised in the form of IUFSU to accommodate such highly massive stars leaving the low density finite nuclear properties unchanged. In this work we have studied this new parameter set in the context of the possibility of having a hyperonic core in such massive stars.

We have included the full octet of baryons in IUFSU. The EoS gets softened due to the inclusion of hyperons whereas the inclusion of the ϕ meson makes the EoS stiffer. We have also investigated the influence of Σ and Ξ potentials on the EoS.

For static stars with hyperonic core we get a maximum mass of $1.62M_{\odot}$. So IUFSU with hyperons cannot reproduce the observed mass of static stars. However, as the observed $\sim 2M_{\odot}$ neutron stars are both pulsars, we compare the results in the rotating limit. In the Keplerian limit we get a maximum mass of $1.93M_{\odot}$, which is within the 3σ limit of the mass of PSR J0348 + 0432 and 1σ limit of the earlier observation of PSR J1614 – 2230. We have looked at the particle densities inside the star

having the maximum mass and found that a considerable amount of hyperons are present near the core. Therefore, our results are consistent with the recent observations of highly massive pulsars confirming the presence of hyperons in the core of such massive neutron stars.

To conclude, IUFSU model, which reproduces the properties of finite nuclei quite successfully also reproduces the recent observations of $\sim 2M_{\odot}$ stars, in case of stars having exotic core and rotating in the Keplerian limit. It will be interesting to see whether such a star can hold a quark core. Related work is in progress.

V. ACKNOWLEDGEMENT

This work is funded by the University Grants Commission (RFSMS, DSKPDF and DRS) and Department of Science and Technology, Government of India.

-
- [1] J. Antoniadis *et al.* *Science* **340**, (2013) 6131.
- [2] P. B. Demorest, T. Pennucci, S. M. Ransom, M. S. E. Roberts and J. W. T. Hessels, *Nature* **467**, (2010) 1081.
- [3] E. Massot, J. Margueron and G. Chanfray, *Eur. Phys. Lett.* **97**, (2012) 39002.
- [4] M. Baldo, G. F. Burgio and H.-J. Schulze, *Phys. Rev. C* **61**, (2000) 055801.
- [5] I. Vidana, A. Polls, A. Ramos, L. Engvik and M. Hjorth-Jensen, *Phys. Rev. C* **62**, (2000) 035801.
- [6] H. Āapo, B.-J. Schaefer and J. Wambach, *Phys. Rev. C* **81**, (2010) 035803.
- [7] J. M. Lattimer and M. Prakash, *From Nuclei to Stars: Festschrift in Honor of Gerald Brown*, p.275, World Scientific, Singapore, (2011).
- [8] N. K. Glendenning *Astrophys. J.* **293**, (1985) 470.
- [9] N. K. Glendenning and S. A. Moszkowski, *Phys. Rev. Lett.* **67**, (1991) 2414.
- [10] R. Knorren, M. Prakash and P. J. Ellis, *Phys. Rev. C* **52**, (1995) 3470.
- [11] S. Balberg and A. Gal, *Nucl. Phys. A* **625**, (1997) 435.
- [12] S. Pal, M. Hanauske, I. Zakout, H. Stöcker and W. Greiner, *Phys. Rev. C* **60**, (1999) 015802.
- [13] M. Hanauske, D. Zschesche, S. Pal, S. Schramm, H. Stöcker and W. Greiner, *Astrophys. J.* **537**, (2000) 958.
- [14] S. Schramm and D. Zschesche, *J. Phys. G* **29**, (2003) 531.
- [15] W. H. Long, B. Y. Sun, K. Hagino and H. Sagawa, *Phys. Rev. C* **85**, (2012) 025806.
- [16] H. Huber, M. K. Weigel and F. Weber, *Z. Naturforsch.* **54A**, (1999) 77.
- [17] F. Hofmann, C. M. Keil and H. Lenske, *Phys. Rev. C* **64**, (2001) 034314.
- [18] J. Rikowska-Stone, P. Guichon, H. Matevosyan and A. Thomas, *Nucl. Phys. A* **792**, (2007) 341.
- [19] S. K. Dhiman, R. Kumar and B. K. Agrawal, *Phys. Rev. C* **76**, (2007) 045801.
- [20] V. Dexheimer and S. Schramm, *Astrophys. J.* **683**, (2008) 943.
- [21] I. Bombaci, P. K. Panda, C. Providencia and I. Vidana, *Phys. Rev. D* **77**, (2008) 083002.
- [22] R. Cavagnoli, D. P. Menezes and C. Providencia, *Phys. Rev. C* **84**, (2011) 065810.
- [23] M. Baldo, G. F. Burgio and H.-J. Schulze, *Phys. Rev. C* **58**, (1998) 3688.
- [24] S. Nishizaki, T. Takatsuka and Y. Yamamoto, *Prog. Theor. Phys.* **108**, (2002) 703.
- [25] H.-J. Schulze, A. Polls, A. Ramos and I. Vidana, *Phys. Rev. C* **73**, (2006) 058801.
- [26] H.-J. Schulze and T. Rijken, *Phys. Rev. C* **84**, (2011) 035801.
- [27] D. Logoteta, I. Vidana, C. Providencia, A. Polls and I. Bombaci, *J. Phys.: Conf. Ser.* **342**, (2012) 012006.
- [28] I. Bednarek, P. Haensel, J. L. Zdunik, M. Bejger and R. Mańka, *Astron. Astrophys.* **543**, (2012) A157.
- [29] R. Lastowiecki, D. Blaschke, H. Grigorian and S. Typel, *Acta Phys. Pol. B Proc. Suppl* **5**, (2012) 535.
- [30] A. R. Taurines, C. A. Z. Vasconcellos, M. Malheiro and M. Chiapparini, *Mod. Phys. Lett. A* **15**, (2000) 1789.
- [31] L. Bonanno and A. Sedrakian, *Astron. Astrophys.* **539**, (2012) A16.
- [32] N. Gupta and P. Arumugam, *Phys. Rev. C* **85**, (2012) 015804.
- [33] B. K. Agrawal, A. Sulaksono and P. -G. Reinhard, *Nucl. Phys. A* **882**, (2012) 1.
- [34] S. Weissenborn, D. Chatterjee and J. Schaffner-Bielich, *Phys. Rev. C* **85**, (2012) 065802.
- [35] B. G. Todd-Rutel and J. Piekarewicz *Phys. Rev. Lett.* **95**, (2005) 122501.
- [36] C. Wu and Z. Ren, *Phys. Rev. C* **83** (2011) 025805.
- [37] F. J. Fattoyev, C. J. Horowitz, J. Piekarewicz and G. Shen, *Phys. Rev. C* **82**, (2010) 055803.
- [38] G. A. Lalazissis, J. König and P. Ring, *Phys. Rev. C* **55**, (1997) 540.
- [39] C. B. Dover and A. Gal, *Prog. Part. Nucl. Phys.* **12**, (1985) 171.
- [40] J. Schaffner, C. B. Dover, A. Gal, C. Greiner, D. J. Mil-

- lener and H. Stöcker, *Annals of Physics* **235**, (1994) 35.
- [41] D. J. Millener, C. B. Dover and A. Gal, *Phys. Rev. C* **38**, (1988) 2700; J. Schaffner, H. Stöcker and C. Greiner, *Phys. Rev. C* **46**, (1992) 322.
- [42] J. Mares, W. Friedman, A. Gal and B. K. Jennings, *Nucl. Phys. A* **594**, (1995) 311.
- [43] J. Schaffner-Bielich and A. Gal, *Phys. Rev. C* **62**, (2000) 034311.
- [44] H. Komatsu, Y. Eriguchi and I. Hachisu, *Monthly Notices of Royal Astronomical Society* **237**, (1989) 355.
- [45] N. Stergioulas and J. H. Friedman, *Astrophys. J.* **444**, (1995) 306.
- [46] B. K. Agrawal, A. Sulaksono, P. -G. Reinhard, *Nucl. Phys. A* **882** (2012) 1.